Study on the Propagation Characteristics of Gold-Silver Hybrid Chain Nanostructures

Shenxiang Yang[1], Dan Zhang[1, *], Huiwen Chen[1], Shuo Wang[1], and Chun-Ping Chen[2, *]

Abstract—In this paper, the transport characteristics of gold/silver mixed chain nanostructures with different proportions of infinite length in the range of 270–810 nm are studied, and the corresponding band gap characteristics and other transport characteristics are analyzed. We introduced an analytical model to determine the complex dielectric constant of an arbitrary composition Au-Ag alloy, and combined this with the experimental data to study the propagation characteristics of the infinite-length gold-silver mixed-chain nanostructures with various compositions. As the gold content exceeds $\text{Au} : \text{Ag}\,(1 : 2)$, the coupling coefficient between the forward and reverse waves becomes smaller, and the reverse wave cannot provide enough energy to transfer to the forward wave. The scattering ability of the scattering unit weakens; the frequency range of the propagation state widens; and it exhibits good propagation characteristics. By gradually increasing the proportion of metal in the alloy, we can explore the variation of the propagation characteristics of the alloy. At present, the change of metal propagation characteristics has not been studied from this point, so we found for the first time that frequency modulation can be realized through this method (regulating the attenuation or cutoff frequency range, namely the band gap range). We also studied a cylindrical finite array chain composed of 40 nanorods under five types of experimental data and discussed the wave guiding ability of the finite array chain under the excitation of a plane wave of a specific wavelength.

1. INTRODUCTION

Photonic crystals are man-made periodic dielectric structures with photonic band-gap (PBG) characteristics. In Twersky's pioneering work published in 1960 [1], he proposed the scattering problem related to infinite gratings of equidistant cylinders through a Fourier series expansion method; in 2002, Krenn et al. proposed the maintenance of collective electronic oscillations. It was thus established that metal nanowires can be used as optical waveguides [2]. In recent years, researchers have made significant efforts toward developing new structures comprising multilayer arrays based on the periodic distribution of photonic crystals. In 2018, Zhang and Zhu increased the phase constant and attenuation constant related to the forward propagation leaky mode, back-propagation leaky mode, and guided mode, and conducted in-depth investigations [3]. The shape of the air hole etched in the photonic crystal waveguide plays a vital role in energy transmission and efficiency. Stronger guided mode interactions can extract low-order modes and improve the efficacy for extracting high-order modes [4]. If electrons propagate in the periodic potential field, the generated electron waves will be scattered according to Bragg's law concerning the periodic potential field; this process generates a unique band structure [5–11]. Gold and silver are common research objects in studies regarding metal photonic crystals. In particular, silver has strong surface plasmon resonance characteristics. It has been determined that the propagation characteristics of silver nanorod arrays exhibit single-frequency and multi-mode phenomena, which can

be used for multi-mode communication [12]. Analyzing the propagation distribution reveals that the state distribution corresponding to distinct frequency bands has guiding significance for the production of various functional devices. Additionally, gold has high chemical stability and can significantly enhance the surface Raman scattering of photonic crystals; however, gold is expensive and exhibits relatively weak surface plasmon resonance [13]. The gold-silver alloy nanostructure embodies strong scattering characteristics, which strengthens the Fano resonance signal of the alloy waveguide coupled photonic crystal relative to that of the pure gold structure. The extinction spectrum of gold and silver alloy structure varies more with the refractive index of environment than that of pure gold, and change is more sensitive [14, 15]. From a structural perspective, a single-stranded waveguide contains a finite or infinite number of coupled nanoparticles arranged at equal distances within an array. Light propagates along the chain of particles due to near-field interactions between nanoparticles. If different frequencies are selected in the distinct Bragg periods of a single structure, the light propagation direction and energy direction are directly proportional and opposite [11]. Because the photonic crystal forbidden band can allow qualified light waves to pass, its forbidden properties can be exploited to design and manufacture photonic crystal filters [16, 17], low-threshold lasers [18–21], and other devices. In particular, the reflectance and transmittance of the filter are related to the number, dielectric constant, and size of the defective rods, and the phenomenon of transmission resonance has emerged in some cases [22].

The present work investigates the complex propagation characteristics of infinitely-long pure silver, gold-silver alloy (with various Au : Ag ratios), and pure gold chain nanostructures in the wavelength range of 270–810 nm. We compare the permittivity of Johnson experimental data with that of Rioux experimental data to evaluate four groups of single-mode transmission generalized multipole technology, Fourier Series Expansion Method (FSEM), and finite time domain difference technology results. The comparative results indicated that the results were generally consistent. The complex propagation characteristics of Au : Ag (1 : 2), Au : Ag (2 : 1), and pure Au chain nanostructures were also evaluated, and an analytical model was introduced to determine the complex permittivity of any Au-Ag alloy composition [23]. Because the gold content does not increase to Au : Ag (1 : 2), the propagation frequency range of the alloy structure is lower than that of the plasma structure composed of silver nanorods array, and the attenuation and cutoff frequency range are wider. As the gold content exceeds Au : Ag (1 : 2), the coupling coefficient between the forward and reverse waves is reduced, and the reverse direction cannot provide enough energy to transfer to the forward wave. Thus, the scattering ability of the scattering unit weakens; the frequency range of the propagation state widens; and it exhibits good propagation characteristics. By gradually increasing the proportion of metal in the alloy, we can explore the variation of the propagation characteristics of the alloy. At present, the change of metal propagation characteristics has not been studied from this point, so we found for the first time that frequency modulation can be realized through this method (regulating the attenuation or cutoff frequency range, namely the band gap range). Our study shows that the band gap range can be adjusted by increasing and decreasing the proportion of gold in the au-ag alloy by adjusting the attenuation frequency range and cutoff frequency.

We also studied a finite array chain composed of 40 nanorods under five types of experimental data and discuss the wave guiding ability of the finite array chain under the excitation of a plane wave of a specific wavelength. By evaluating the properties of waveguides at specific wavelengths, various stages can be applied to different devices.

2. STATEMENT OF THE PROBLEM

In this section, we will introduce the specific application of Fourier Series Expansion Method (FSEM) in this study. The two-dimensional infinite periodic chain consists of cylinders arranged periodically along the x-axis, with a lattice constant h (Fig. 1). Each column is evenly spaced and made of gold and silver alloy, and the rest of the blank space is air. In the z direction, the scattering element cylinders are infinitely long and distributed parallel to each other.

We assume that a cylinder with a bottom radius of r is a pure dielectric, with a dielectric constant of ε. An array with this structure repeats the same configuration along the y-direction, assuming that the period is Λ, and then the cells in the array with $0 \leq y \leq \Lambda$ are used to approximate the initial structure. Suppose that we guide the propagation of waves. For clarity and simplicity, herein we omit the details
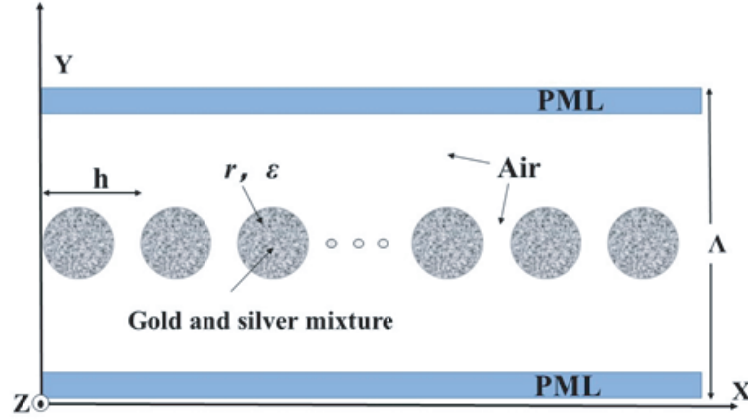
Figure 1. An infinite periodic chain of annular rods along the x-axis, with a lattice constant h. The radius and dielectric constant of the rod are r and ε, respectively.

of the formulation and direct interested readers to our group's previous work [24, 25] for further details. Surface plasmons occur at the metal-medium interface, and they are collectively vibrated by a large number of free electrons excited only by H (the magnetic field component perpendicular to the cross-section of the nanowire) [26]. First, we describe the core content of the formulation. For H waves, Maxwell's equation is given as follows,

$$G\left(y\right)\frac{\partial H'}{\partial y} = ik_0\varepsilon\left(y\right)E_x, \tag{1}$$

$$-\frac{\partial H'_z}{\partial x} = ik_0\varepsilon\left(y\right)E_y = ik_0\frac{D_y}{\varepsilon_0} \tag{2}$$

$$\frac{\partial E_y}{\partial x} - G\left(y\right)\frac{\partial E_x}{\partial y} = -ik_0H', \tag{3}$$

$$D_y = \varepsilon_0\varepsilon\left(y\right)E_y. \tag{4}$$

where $H' = (\mu_0/\varepsilon_0)^{1/2}H_z$; $G(y) = [1 + i\sigma(y)]^{-1}$ is the stretch coordinate variable [27], which represents the hypothetical perfect matching layer (PML); $\sigma(y) = \sigma_{\max}(1 - y/\omega)^d$ is the conductivity function. In the virtual period of the propagation field, the electric and magnetic fields are approximated as truncated Fourier series, as shown in Eqs. (5)–(8),

$$H'(x,y) = \sum_{m=-M}^{M} h_{z,m}\left(x\right)e^{i\varphi_m y}, \tag{5}$$

$$E_x(x,y) = \sum_{m=-M}^{M} e_{x,m}\left(x\right)e^{i\varphi_m y}, \tag{6}$$

$$E_y(x,y) = \sum_{m=-M}^{M} e_{y,m}\left(x\right)e^{i\varphi_m y}, \tag{7}$$

$$D_y(x,y) = \sum_{m=-M}^{M} d_{y,m}\left(x\right)e^{i\varphi_m y}. \tag{8}$$

where D_y is the electric displacement vector, and $\varphi_m = 2\pi m/\Lambda$. Next, Eq. (2) is substituted into Eq. (1), to perform calculations according to the orthogonal property of a Fourier basis. Some H modes have characteristics of the field component (H_z, E_x, E_y), and we set H_z as the dominant field. There is a problem of discontinuity in the electric field perpendicular to the boundary of the core and cladding. To

solve this problem, we refer to Li's decomposition rule [28] and expand the field of E_y via Fourier series. This enables the derivation of a set of linear equations to determine the Fourier coefficients $\{h_{z,m}(x)\}$ and $\{e_{y,m}(x)\}$,

$$\frac{\partial^2}{\partial x^2} h_z(x) = -k_0 G \cdot h_z(x), \tag{9}$$

$$e_y(x) = -i \frac{1}{k_0} \hat{N} \cdot \frac{\partial}{\partial x} h_z(x), \tag{10}$$

$$h_z(x) = [h_{z,-M} \ldots h_{z,0} \ldots h_{z,M}]^T \tag{11}$$

$$e_y(x) = [e_{y,-M} \ldots e_{y,0} \ldots e_{y,M}]^T \tag{12}$$

$$G = \hat{N}^{-1} \left(1 - VAN^{-1}VA\right), \tag{13}$$

$$[N]_{mm'} = \frac{1}{\Lambda} \int_0^\Lambda \varepsilon(y) e^{-i(\varphi_m - \varphi_{m'})y} dy, \tag{14}$$

$$\left[\hat{N}\right]_{mm'} = \frac{1}{\Lambda} \int_0^\Lambda \frac{1}{\varepsilon(y)} e^{-i(\varphi_m - \varphi_{m'})y} dy, \tag{15}$$

$$[V]_{mm'} = \frac{1}{\Lambda} \int_0^\Lambda \nu(y) e^{-i(\varphi_m - \varphi_{m'})y} dy, \tag{16}$$

$$[A]_{mm'} = \frac{\phi_m}{k_0} \delta_{mm'}. \tag{17}$$

where $\delta_{mm'}$ is the Kronecker delta; the superscript T indicates the transpose of the vector; k_0 is the wave number in free space; $\varepsilon(y)$ is the dielectric constant along the y-axis in a period of $0 \leq y \leq \Lambda$. $\nu(y) = 1/[1 + i\sigma(y)]$ represents the tensile coordinate variable PML parameter related to the coordinate system. The eigenvalue $k_n = \xi_n$ $(n = 1, 2, 3, \ldots, 2M + 1)$ of the matrix G determines the propagation constant ξ_n and the guided mode in the hypothetical waveguide. The characteristic vector P_n determines the field distribution of the radiation pattern. The solutions of Eqs. (8) and (9) are given as follows,

$$\begin{bmatrix} h_z(x) \\ e_y(x) \end{bmatrix} = F_H u(x - x') \cdot a(x'), \tag{18}$$

$$F_H = \begin{bmatrix} P & P \\ \hat{N}PB & -\hat{N}PB \end{bmatrix}, \tag{19}$$

$$u(x) = \begin{bmatrix} u^{(+)}(x) & 0 \\ 0 & u^{(-)}(x) \end{bmatrix}, \tag{20}$$

$$P = [p_1 \ p_2 \ \ldots p_(2M + 1)], \tag{21}$$

$$u^{(\pm)}(x) = [\exp(\pm i k_0 \xi_n x) \delta_{nn'}], \tag{22}$$

$$B = [\xi_n \delta_{mm'}], \tag{23}$$

$$a(x) = \begin{bmatrix} a^{(+)}(x) \ a^{(-)}(x) \end{bmatrix}, \tag{24}$$

$$a^\pm(x) = [a_1^\pm(x) \ a_2^\pm(x) \ \ldots \ a_{2M}^\pm(x) \ a_{2M+1}^\pm]. \tag{25}$$

where $a_n(x)$ represents the amplitude of the n-th order mode of the forward and backward waves. The $u(x)$, P, and $a^{(\pm)}(x)$ terms are rearranged in the order of guidance and radiation patterns, with $\mathrm{Re}[\xi_n]$ decreasing.

Then, as shown in Fig. 2, each cylinder is subdivided into 20 parallel rectangular columns, and the scattering elements of the x-direction periodic chain are replaced by cascades of layered parallel planar waveguides [25].

To compute each section of the waveguide, the solutions of Eqs. (1)–(8) are obtained by using Eqs. (18)–(25). We equalize the Fourier coefficients on both sides of the section, so that H_z and E_y meet the boundary conditions at each step discontinuity. This causes the scattering matrix S_j to adopt
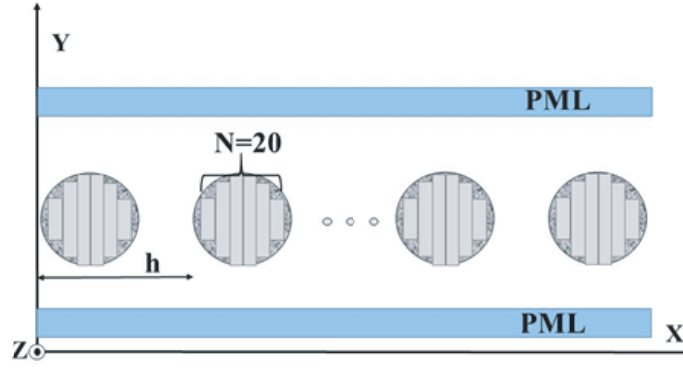
Figure 2. Discrete round rods with a sufficient number of thin, parallel, rectangular rods.

the following relationship at the interface $x=x_j$:

$$\begin{bmatrix} a_{j-1}^{(-)}(x_j - 0) \\ a_j^{(+)}(x_j + 0) \end{bmatrix} = S_j \begin{bmatrix} a_{j-1}^{(+)}(x_j - 0) \\ a_j^{(-)}(x_j + 0) \end{bmatrix}, \tag{26}$$

$$S_j = \begin{bmatrix} R_j^{(-)} & T_j \\ T_j & R_j^{(+)} \end{bmatrix}$$

$$= \begin{bmatrix} P_{j-1} & -P_j \\ P_{j-1}B_{j-1} & P_jB_j \end{bmatrix}^{-1} \begin{bmatrix} -P_{j-1} & P_j \\ P_{j-1}B_{j-1} & P_jB_j \end{bmatrix} \tag{27}$$

The method used to define the scattering matrix S_{j+1} at $x=x_{j+1}$ is the same as that shown in Eq. (25). In addition, we must consider the modal propagation at a distance $x_{j+1}-x_j$, as follows,

$$S_{j+1} = \begin{bmatrix} R_{j+1}^{(-)} & T_{j+1} \\ T_{j+1} & R_{j+1}^{(+)} \end{bmatrix}, \tag{28}$$

And

$$\hat{R}_{j+1}^{(-)} = \hat{R}_j^{(-)} + \hat{T}_j X_{j+1} u_j^{(+)} R_{j+1}^{(-)} u_j^{(+)} \hat{T}_j, \tag{29}$$

$$\hat{T}_{j+1} = T_j u_j^{(+)} Y_{j+1} \hat{T}_j, \tag{30}$$

$$\hat{R}_{j+1}^{(+)} = \hat{R}_{j+1}^{(-)} + \hat{T}_{j+1} u_j^{(+)} Y_{j+1} \hat{R}_j^{(+)} u_j^{(+)} \hat{T}_{j+1}, \tag{31}$$

$$X_{j+1} = \left(I - u_j^{(+)} R_{j+1}^{(-)} u_j^{(+)} \hat{R}_j^{(+)} \right)^{-1}, \tag{32}$$

$$Y_{j+1} = \left(I - \hat{R}_{j+1}^{(+)} u_j^{(+)} R_j^{(-)} u_j^{(+)} \right)^{-1}, \tag{33}$$

$$u_j^{(+)} = u^{(+)}(x_{j+1} - x_j). \tag{34}$$

where I is the identity matrix; $u^{(+)}(x)$ is defined by Eq. (22). The recursive relation of scattering matrix of waveguide at each discontinuous point can be expressed by Eqs. (29)–(31). When the light is constantly changing in the propagation process of the waveguide, the transition section is approximately a large number of step discontinuities. If it exists along the waveguide at $x=x_j$ $(j = 1, 2, \ldots, N)$, the $(N-1)$ times recursive process will make the generalized scattering matrix S_N [25] of the entire system as:

$$\begin{bmatrix} a_1^{(-)}(x_1 - 0) \\ a_N^{(+)}(x_N + 0) \end{bmatrix} = S_N \begin{bmatrix} a_1^{(+)}(x_1 - 0) \\ a_N^{(-)}(x_N + 0) \end{bmatrix}. \tag{35}$$

In each period h, we calculate the generalized scattering matrix in the x-direction according to the relationship in Eq. (35), where N represents the number of small rectangles in the cell. According to the calculated results, a transition matrix K conforming to the following relationship [25] is obtained:

$$\begin{bmatrix} a^+ (h) \\ a^- (h) \end{bmatrix} = K_N \begin{bmatrix} a^+ (0) \\ a^- (0) \end{bmatrix}. \tag{36}$$

Therefore, the propagation constant $\gamma_k = \beta_k + i\alpha_k$ of the k-th mode is determined by Eq. (37),

$$\gamma_k = -i \log \chi_k / h. \tag{37}$$

where the k-th eigenvalue of the transfer matrix K_N is χ_K. According to Floquet's theorem, the propagation constant β_K of the k-th guided mode can be determined by the following relationship:

$$\chi_k = \exp(i\beta_k h). \tag{38}$$

3. RESULTS AND DISCUSSION

This section first compares the complex propagation constant curve trends of the four methods and discusses the characteristics of the four results. The four methods are: FSEM method from Johnson experimental data FSEM(J), FSEM method from Rioux experimental data FSEM(R), finite difference time domain method FDTD(R) from Rioux experimental data, and generalized multipole technology GMT(J) from Johnson experimental data [23]. The end results are similar.

This paper mainly uses FDTD method (blue line) to verify. However, FDTD method is not accurate enough in calculating the complex propagation constant of the structure, so the results are consistent with FSEM method only in the first half. (FDTD method is used to study the complex propagation constant of gold and silver alloy chain structure, and the research results are only consistent with FSEM method in the first half.) The results can still prove the effectiveness of Rioux experimental data and the FSEM. The radius of the metal circle of the scattering unit is 25 nm, and the period length h is 55 nm. We assume that the period Λ is 60 h, the cut-off number $M = 150$; the number of parallel thin rectangles in each cell is 20; the thickness of the PML $= h$, and $d = 2.1$. The wavelength range of the experimental data was 270–810 nm, and the results are presented in Fig. 3.

According to Fig. 3, the results obtained using the two sets of experimental data are very similar. Ag(FSEM)(J) represents the experimental results concerning the permittivity of the Johnson experimental data, and Ag(FSEM)(R) represents the results from investigating the permittivity of
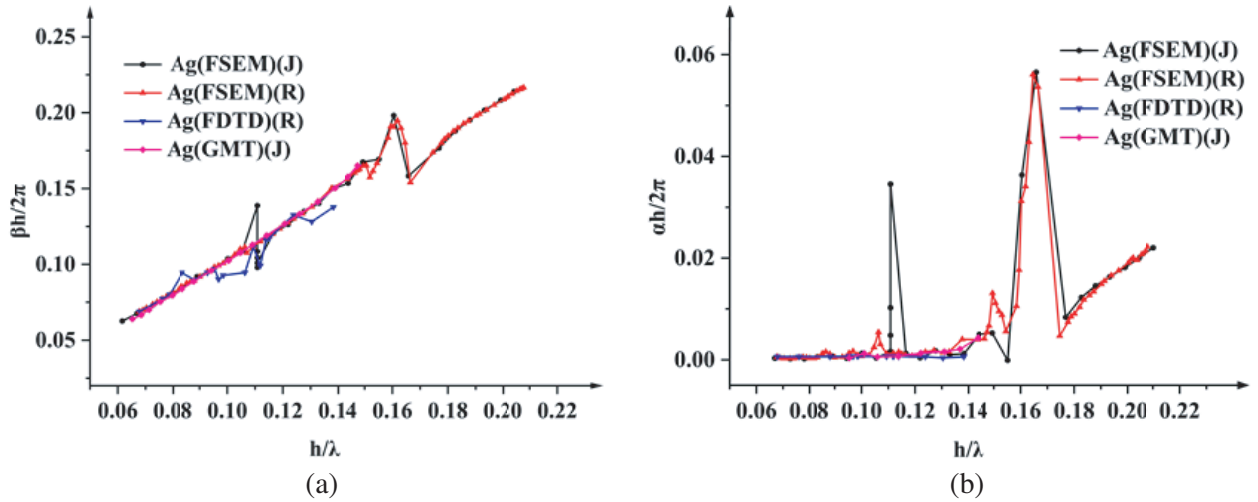
Figure 3. Analysis of the phase constant and attenuation constant of the infinitely-long silver nanorod array with $r = 25$ nm, $h = 55$ nm. The figure shows the dielectric functions: (a) phase constant; (b) attenuation constant.

the Rioux experimental data. It is evident that the phase constant and attenuation constant change suddenly at the frequencies of 0.11 and 0.166. The first abrupt change was caused by a multimode band. The multimode band does not emerge in the Rioux experimental data calculation because the data corresponding to a wavelength of 496 nm cannot be obtained. The second abrupt change of curve was caused by the abrupt change and structure of the dielectric constant [12].

The propagation properties of Au : Ag (1 : 4) chain nanostructures were studied using the parametric model in the appendix, and the propagation properties of pure Au, Au : Ag (1 : 2) and Au : Ag (2 : 1) were also studied using Rioux experimental data. We used the same parameter settings to study the characteristics of pure Au, Au : Ag (1 : 2), Au : Ag (2 : 1), and the multi-parameter model of the complex propagation constant of Au : Ag (1 : 4) chain nanostructures under the Rioux experimental data. Fig. 4 shows the numerical changes in the phase constant and attenuation constant with frequency, combined with previous research results involving pure Ag under Rioux experimental data.
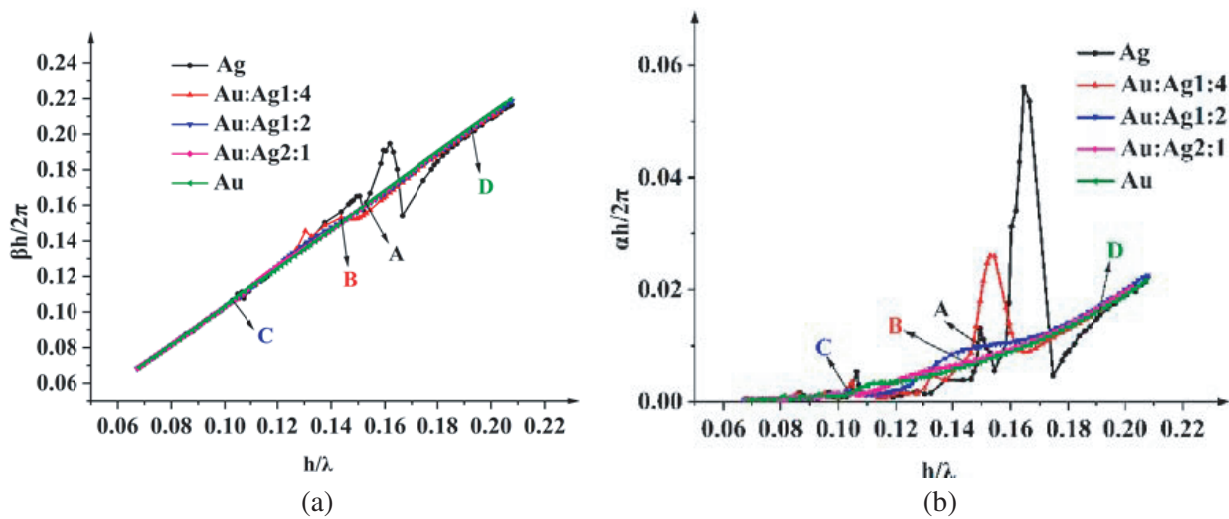
Figure 4. Analysis of the phase constants and attenuation constants of the five compositions of metal nanorod arrays. The figure shows the dielectric function: (a) phase constant; (b) attenuation constant.

It can be seen from Figure 4 that the phase constant and attenuation constant have the largest overall fluctuation with frequency. The frequencies of point A-D are 0.1532, 0.1437, 0.1037, and 0.1909. With the increase of gold content in the alloy, the phase constant and attenuation constant change curves with frequency tend to be gentle. This means that in the propagation frequency range, the smaller the energy loss is, the higher the transmission power is. As the gold content in the alloy increases, the reverse wave gradually decreases, and the forward wave cannot transfer enough energy for exchange, so the scattering ability of the scattering unit is weakened. This observation lays the foundation for subsequent research regarding the characteristics and practical value of the mixed-chain nanostructures with limited and varying proportions of gold and silver.

To study the wave guiding ability of a finite alloy array chain comprising various Au/Ag proportions under the excitation of a plane wave of a specific wavelength, a cylindrical finite array chain composed of 40 nanorods was selected as the object of study. Through a large number of simulation experiments and literature comparison, it is found that in the transmission process of light, the attenuation state or cutoff state begins at the place where the attenuation coefficient rises with the initial frequency curve. The special frequency points we choose are all taken from the initial rising frequency point or the frequency points after the initial rising frequency point. Through the test of each frequency point, the result in Table 1 is obtained.

We find that when the content of gold in the alloy chain nanostructure is low, the frequency range of the propagation state is lower than that of the pure silver chain nanostructure. As the gold content

Table 1. Chain structure propagation characteristics of different proportions of metals.

Material	propagation stage	Attenuated or Cut-off state
Ag	$h/\lambda < 0.144$	$h/\lambda > 0.144$
Au : Ag 1 : 4	$h/\lambda < 0.13$	$h/\lambda > 0.13$
Au : Ag 1 : 2	$h/\lambda < 0.178$	$h/\lambda > 0.178$
Au : Ag 2 : 1	$h/\lambda < 0.182$	$h/\lambda > 0.182$

in the alloy increases, the frequency range of the propagation state gradually increases and exceeds that of the pure silver chain nanostructure; meanwhile, the frequency range of the attenuation or cut-off state gradually decreases. By gradually increasing the proportion of a metal in the alloy, we can explore the changing law of the propagation characteristics of the alloy. At present, there is no research on the variation of metal propagation characteristics from this point, so we are the first to find that we can achieve frequency modulation (regulating the attenuation or cutoff frequency range, i.e., the band gap range) method through this method.

In order to provide a more comprehensive analysis, the field distribution and propagation distribution of several different and representative frequency points were evaluated at different stages. Fig. 5–Fig. 8 are respectively taken from A-D frequency points. In the finite array of pure silver chain nanostructures, when $h/\lambda = 0.149$ ($\lambda = 359$ nm), it is the point where the attenuation constant value of the second abrupt change is the largest. At this frequency, the light changes from the attenuation state to the completely cut-off state, and the light cannot propagate in this structure, as shown in Figs. 5(a) and (b). In the Au : Ag (1 : 4) chained nanostructure finite array, when $h/\lambda = 0.144$ ($\lambda = 383$ nm), it is a frequency point before the second abrupt change. At this frequency, the propagation distribution is weakened, and the light is in a state of attenuation, as shown in Figs. 6(a) and (b). In the Au : Ag (1 : 2) chained nanostructure finite array, $h/\lambda = 0.104$ ($\lambda = 530$ nm) is taken as the representative point of the low frequency point. At this frequency, the light spreads forward uniformly and has low loss, which can be used in waveguides or sensors, as shown in Figs. 7(a) and (b). In the finite array of pure Au chain nanostructures, $h/\lambda = 0.191$ ($\lambda = 288$ nm) is taken as the representative point of the high frequency

(a)   (b)
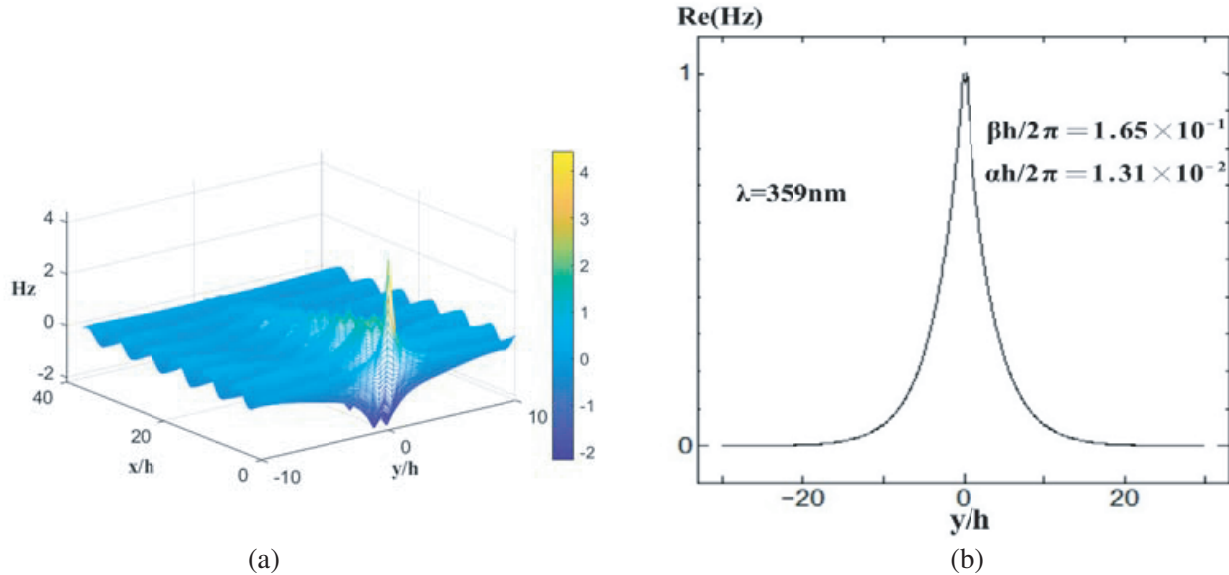
Figure 5. (a) Near-field propagation distribution of the silver chain structure at a wavelength of 359 nm; (b) distribution of the Hz field along the y-axis of the silver chain structure at a wavelength of 359 nm.

point. At this frequency, the propagation of light is completely cut off, as shown in Figs. 8(a) and (b). We have found that with the rational use of the characteristics the high-frequency cut-off state is beneficial to our production of various filters and photonic crystal mirrors, etc., which has laid the theoretical foundation for our subsequent research and application.

(a)   (b)
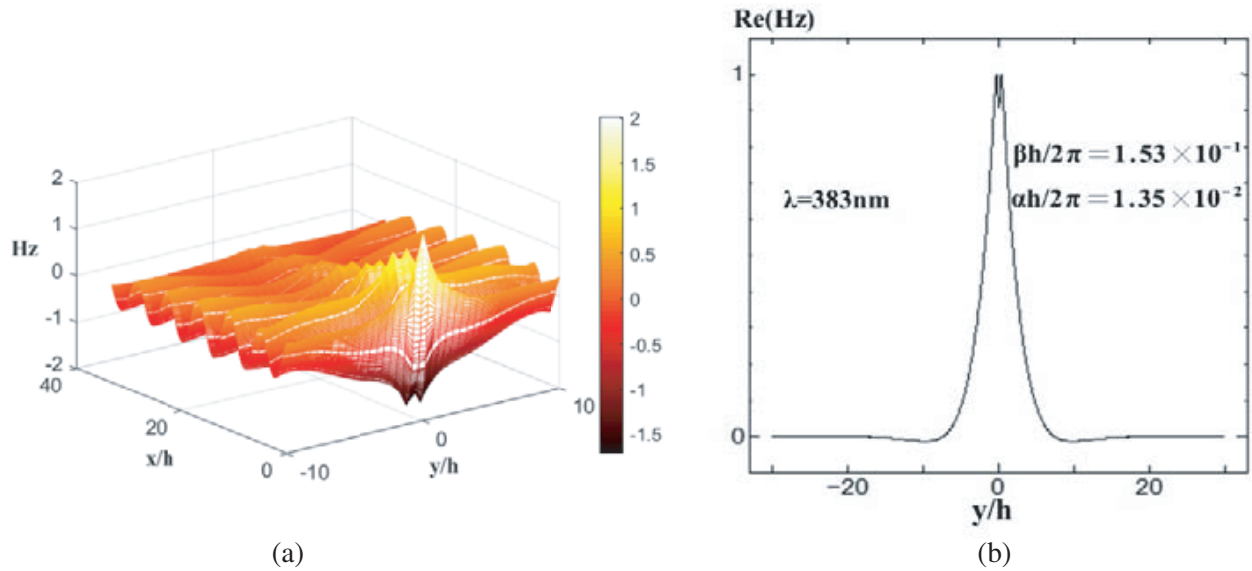
Figure 6. (a) Near-field propagation distribution of the Au : Ag (1 : 4) chain structure with a wavelength of 383 nm; (b) distribution of the Hz field along the y-axis of the Au : Ag (1 : 4) chain structure with a wavelength of 383 nm.

(a)   (b)
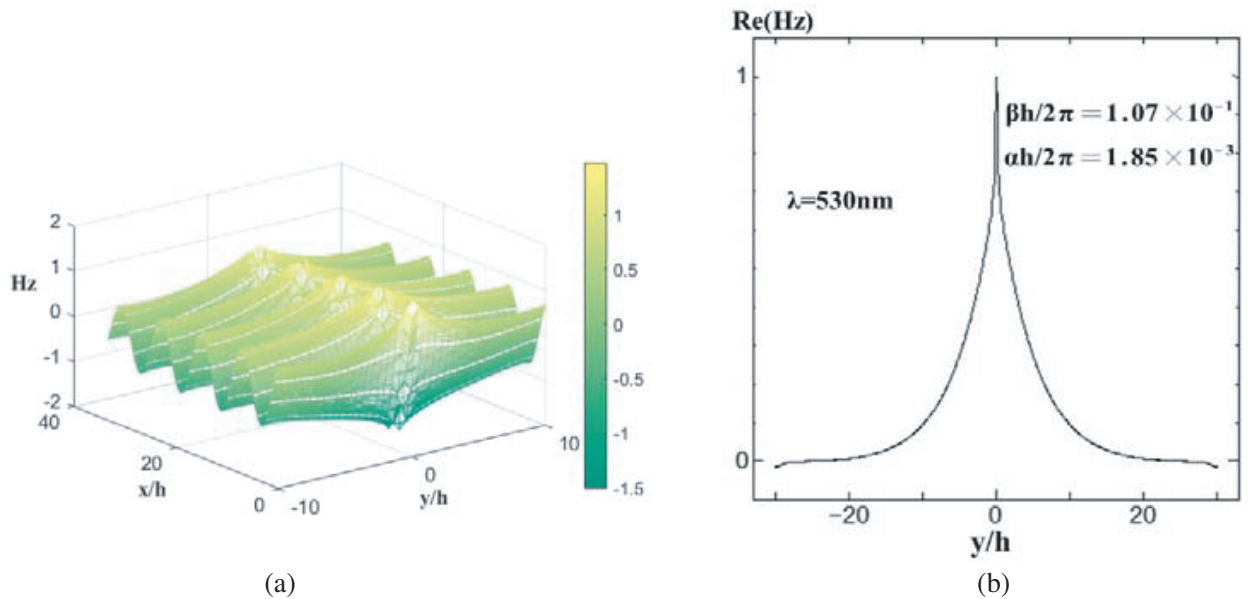
Figure 7. (a) Near-field propagation distribution of the Au : Ag (1 : 2) chain structure with a wavelength of 530 nm; (b) distribution of the Hz field along the y-axis of the Au : Ag (1 : 2) chain structure with a wavelength of 530 nm.
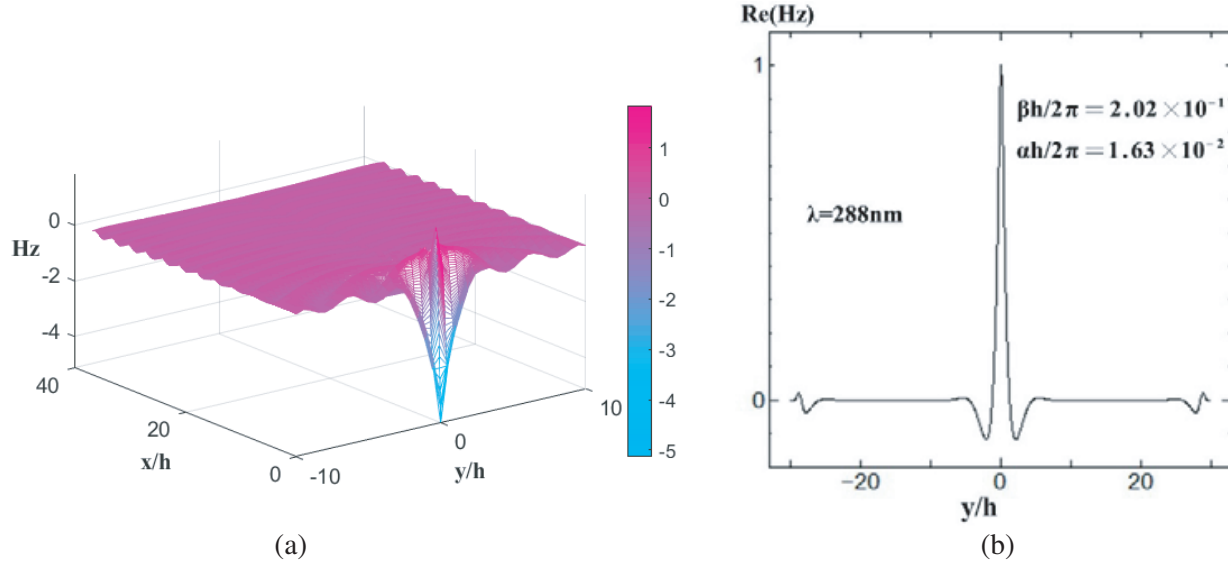
Figure 8. (a) Near-field propagation distribution of pure gold chain nanostructures at a wavelength of 288 nm; (b) Hz field distribution along the y-axis of pure gold chain nanostructures at a wavelength of 288 nm.

4. CONCLUSION

This study employs two types of data and three research methods to investigate the complex propagation constants of infinite pure silver chain nanostructures in the range of 270–810 nm and analyze the characteristics of the complex propagation constant. The characteristics of the complex propagation constants of pure Au, Au : Ag (1 : 4), Au : Ag (1 : 2), and Au : Ag (2 : 1) chain nanostructures were also studied based on the Rioux experimental data. As the gold content exceeds Au : Ag (1 : 2), the coupling coefficient between the forward and reverse waves decreased, and the reverse wave could not provide enough energy to transfer to the forward wave. The scattering ability of the scattering unit became weaker; the frequency range of the propagation state became wider; and it exhibited good propagation characteristics. We used a cylindrical finite array chain composed of 40 nanorods as the object of study to study the propagation distribution of this structure. By gradually increasing the proportion of a metal in the alloy, we can explore the changing law of the propagation characteristics of the alloy. At present, there is no research on the variation of metal propagation characteristics from this point, so we are the first to find that we can achieve frequency modulation (regulating the attenuation or cutoff frequency range, i.e., the band gap range) method through this method. It can be seen from our research results that the range of attenuation and cut-off frequency can be controlled by adjusting the proportion of gold in the au-ag alloy, and thus the range of forbidden band can be controlled. In the range of propagation frequency, the higher the content of gold is in the alloy, the smoother the curve of attenuation constant with frequency is, that is, the smaller the loss in the process of adjusting the change of wavelength is. This will give the engineering community a new direction in making filters, photonic crystal reflectors, and antennas. By studying the properties of waveguides at specific wavelengths, distinct stages can be applied to different devices. The propagation frequency range can be used for waveguides and sensors, and the cut-off frequency band can be used for filters and mirrors.

APPENDIX A.

We evaluated the characteristics of the complex propagation constant of the $\mathrm{Au} : \mathrm{Ag}\,(1 : 4)$ chain structure under the Rioux experimental data for pure Au, $\mathrm{Au} : \mathrm{Ag}\,(1 : 2)$, $\mathrm{Au} : \mathrm{Ag}\,(2 : 1)$, and multi-parameter model calculations. We used an arbitrary composition of the Au-Ag alloy for complex permittivity analysis to characterize the optical dielectric function $\varepsilon(\omega)$ of the gold-silver alloy nanowires and obtained the optimized fitting of the gold-silver alloy dispersion [23]. The shape of JDOS (Joint Density Of States) is the core element that affects the shape of the dielectric function, and the critical point is the main factor that affects JDOS itself. Here, we used a parabola to approximate the gap energy near the critical point. The band-to-band contribution of the critical point to the dielectric function is given by Eq. (A1):

$$\varepsilon_{cp1}(\omega) = A\left[-\frac{\sqrt{\omega_{g1}-\omega_{01}}}{2(\omega+i\Gamma_1)^2}\ln\left(1-\left(\frac{\omega+i\Gamma_1}{\omega_{01}}\right)^2\right) + \frac{2\sqrt{\omega_{g1}}}{(\omega+i\Gamma_1)}\tanh^{-1}\left(\sqrt{\frac{\omega_{g1}-\omega_{01}}{\omega_{g1}}}\right)\right.$$
$$\left.-\frac{\sqrt{\omega+i\Gamma_1-\omega_{g1}}}{(\omega+i\Gamma_2)^2}\tan^{-1}\left(\sqrt{\frac{\omega_{g1}-\omega_{01}}{\omega+i\Gamma_1-\omega_{g1}}}\right)-\frac{\sqrt{\omega+i\Gamma_1+\omega_{g1}}}{(\omega+i\Gamma_1)^2}\tanh^{-1}\left(\sqrt{\frac{\omega_{g1}-\omega_{01}}{\omega+i\Gamma_1+\omega_{g1}}}\right)\right] \quad (A1)$$

The band-to-band contribution of the critical point A to the dielectric function is expressed as shown in Eq. (A2):

$$\varepsilon_{cp2}(\omega) = -\frac{A_2}{2(\omega+i\Gamma_2)^2}\ln\left(1-\left(\frac{\omega+i\Gamma_2}{\omega_{02}}\right)^2\right), \quad (A2)$$

An analytical model of the complex permittivity of an Au-Ag alloy with an arbitrary composition is given by Eq. (A3),

$$\varepsilon(\omega,GMF)=\varepsilon_\infty(GMF)-\frac{(\omega_p(GMF)^2)}{\omega^2+i\omega\Gamma_p(GMF)}+\varepsilon_{cp1}(\omega,\omega_{01}(GMF),\omega_{g1}(GMF),\Gamma_1(GMF),A_1(GMF))$$
$$+\varepsilon_{cp2}(\omega,\omega_{02}(GMF),_2(GMF),A_2(GMF)). \quad (A3)$$

where Γ_1 and Γ_2 are the stretching factors caused by scattering; ω_{01} and ω_{02} are thresholds; ω_{g1} is the gap; A, A_1, and A_2 are the amplitude parameters, including various constants and matrix elements; ε_∞ is the contribution of the high-energy transition; ω_p is the plasma frequency; Γ_p is the Drude broadening factor, which is related to the lifetime of free electrons in the model; GMF is the gold mole fraction. Any given parameter in this equation is closely related to the combination. Research has shown that there are many adequate methods to evaluate parabolic combinatorial correlations, and each method requires three reference points. We chose to refer to the pure composition of Au and Ag, and the midpoint

Table A1. Fitting parameters for the dielectric function of Au-Ag alloys.

	Au	Au Ag 1 : 1	Ag
ω_p [eV]	8.9234	9.0218	8.5546
Γ_p [eV]	0.042389	0.16713	0.022427
ε_∞	2.2715	2.2838	1.7381
ω_{g1} [eV]	2.6652	3.0209	4.0575
ω_{01} [eV]	2.3957	2.7976	3.9260
Γ_1 [eV]	0.1788	0.18833	0.017723
A_1	73.251	22.996	51.217
ω_{02} [eV]	3.5362	3.3400	4.1655
Γ_2 [eV]	0.35467	0.68309	0.18819
A_2	40.007	57.540	30.770

composition of the same amount of Au and Ag. For example, we can use Eq. (A4) to calculate the stretching factor related to the free electron lifetime in the Drude model under any GMF value,

$$\Gamma_p(GMF) = GMF^2(2\Gamma_{pAu} - 4\Gamma_{pAuAg11} + 2\Gamma_{pAg}) + GMF(-\Gamma_{PAu} + 4\Gamma_{pAuAg11} - 3\Gamma_{pAg}) + \Gamma_{pAg}. \quad \text{(A4)}$$

where Γ_{pAu}, $\Gamma_{pAuAg11}$, and Γ_{Ag} are the stretching factors related to the free electron lifetime in the Drude model of pure Au, Au : Ag (1 : 1) alloy, and pure Ag, respectively. Other fitting parameters can also be calculated according to this relationship. We note that the selection of Au, Ag, and Au : Ag (1 : 1) alloy compositions to define the parabola was simply for convenience. The parameters listed in Table A1 were used for these calculations.

REFERENCES

1. Twersky, V., "On scattering of waves by the infinite grating of circular cylinders," *I.R.E. Transactions on Antennas and Propagation*, Vol. 10, No. 6, 737–765, 1962.

2. Krenn, J. R., B. Lamprecht, H. Ditlbacher, G. Schider, M. Salerno, et al., "Non diffraction-limited light transport by gold nanowires," *Europhysics Letters*, Vol. 60, No. 5, 663–669, 2002.

3. Zhang, D. and J. Zhu, "Bi-directional propagation leaky modes in a periodic chain of dielectric circular rods," *Optics Express*, Vol. 26, No. 7, 8690–8698, 2018.

4. Poushimin, R. and T. Jalali, "Radiation losses in photonic crystal slab waveguide to enhance LEDs efficiency," *Superlattices and Microstructures*, Vol. 122, 426–433, 2018.

5. Zhang, D., V. Jandieri, and K. Yasumoto, "Modal analysis of wave guidance by a periodic chain of circular rods," *2016 Progress In Electromagnetics Research Symposium (PIERS)*, Shanghai, China, Aug. 8–11, 2016.

6. Benisty, H., "Modal analysis of optical guides with two-dimensional photonic band-gap boundaries," *Journal of Applied Physics*, Vol. 79, No. 10, 7483–7492, 1996.

7. Yasumoto, K., H. Jia, and K. Sun, "Rigorous modal analysis of two-dimensional photonic crystal waveguides," *Radio Science*, Vol. 40, No. 6, 2005.

8. Xu, Y., R. K. Lee, and A. Yariv, "Adiabatic coupling between conventional dielectric waveguides and waveguides with discrete translational symmetry," *Optics Letters*, Vol. 25, No. 10, 755–757, 2000.

9. Happ, T. D., M. Kamp, and A. Forchel, "Photonic crystal tapers for ultracompact mode conversion," *Optics Letters*, Vol. 26, No. 14, 1102–1104, 2001.

10. Talneau, A., P. Lalanne, M. Agio, and C. M. Soukoulis, "Low-reflection photonic-crystal taper for efficient coupling between guide sections of arbitrary widths," *Optics Letters*, Vol. 27, No. 17, 1522–1524, 2002.

11. Zong, C., D. Zhang, Z. Ding, and Y. Liu, "Mixed propagation modes in three bragg propagation periods of variable chain structures," *IEEE Transactions on Antennas and Propagation*, Vol. 68, No. 1, 311–318, 2020.

12. Zong, C. and D. Zhang, "Analysis of propagation characteristics along an array of silver nanorods using dielectric constants from experimental data and the Drude-Lorentz model," *Electronics*, Vol. 8, No. 11, 2019.

13. Klimonsky, S., A. Baranchikov, V. N. Lad, E. Eremina, A. Garshev, et al., "Photonic and plasmonic effects in inverse opal films with Au nanoparticles," *Photonics and Nanostructures-Fundamentals and Applications*, Vol. 43, 2021.

14. Mu, Y., H. Liu, H. Li, J. Han, C. Huang, et al., "Sensing characteristics of the Gold-Silver alloy nanoparticles assembled waveguided metallic photonic crystals," *Rare Metal Materials and Engineering*, Vol. 48, No. 9, 2879–2884, 2019.

15. Yasli, A. and H. Ademgil, "Effect of plasmonic materials on photonic crystal fiber based surface plasmon resonance sensors," *Modern Physics Letters B*, Vol. 33, No. 13, 2019.

16. Djavid, M. and M. S. Abrishamian, "Multi-channel drop filters using photonic crystal ring resonators," *Optik*, Vol. 123, No. 2, 167–170, 2012.

17. Feng, S. and Y. Wang, "Unidirectional wavelength filtering characteristics of the two-dimensional triangular-lattice photonic crystal structures with elliptical defects," *Optical Materials*, Vol. 35, No. 12, 2166–2170, 2013.

18. Shi, L., F. Jin, M. Zheng, X. Dong, W. Chen, et al., "Low threshold photonic crystal laser based on a Rhodamine dye doped high gain polymer," *Physical Chemistry Chemical Physics*, Vol. 18, No. 7, 5306–5315, 2016.

19. Takiguchi, M., H. Taniyama, H. Sumikura, M. D. Birowosuto, E. Kuramochi, et al., "Systematic study of thresholdless oscillation in high-β buried multiple-quantum-well photonic crystal nanocavity lasers," *Optics Express*, Vol. 24, No. 4, 3441, 2016.

20. Weng, G., Y. Mei, J. Liu, W. Hofmann, L. Ying, et al., "Low threshold continuous-wave lasing of yellow-green InGaN-QD vertical-cavity surface-emitting lasers," *Optics Express*, Vol. 24, No. 14, 15546–15553, 2016.

21. Zhang, T., C. Zhou, W. Wang, and J. Chen, "Generation of low-threshold optofluidic lasers in a stable Fabry-Perot microcavity," *Optics and Laser Technology*, Vol. 91, 108–111, 2017.

22. Rahbarihagh, Y., F. Kalhor, J. Rashed-Mohassel, and M. Shahabadi, "Modal analysis for a waveguide of nanorods using the field computation for a chain of finite length," *Applied Computational Electromagnetics Society Journal*, Vol. 29, No. 2, 140–148, 2014.

23. Rioux, D., S. Vallieres, S. Besner, P. Munoz, E. Mazur, et al., "An analytic model for the dielectric function of Au, Ag, and their alloys," *Advanced Optical Materials*, Vol. 2, No. 2, 176–182, 2014.

24. Jia, H. T., D. Zhang, and K. Yasumoto, "Fast analysis of optical waveguides using an improved fourier series method with perfectly matched layer," *Microwave and Optical Technology Letters*, Vol. 46, No. 3, 263–268, 2005.

25. Zhang, D. and H. Jia, "Numerical analysis of leaky modes in two-dimensional photonic crystal waveguides using Fourier series expansion method with perfectly matched layer," *IEICE Trans. Electron.*, Vol. 90, 613–622, 2007.

26. Barnes, W. L., A. Dereux, and T. W. Ebbesen, "Surface plasmon subwavelength optics," *Nature*, Vol. 424, No. 6950, 824–830, 2003.

27. Wuenschell, J. and H. K. Kim, "Excitation and propagation of surface plasmons in a metallic nanoslit structure," *IEEE Transactions on Nanotechnology*, Vol. 7, No. 2, 229–236, 2008.

28. Li, L. F., "Use of Fourier series in the analysis of discontinuous periodic structures," *Journal of the Optical Society of America A — Optics Image Science and Vision*, Vol. 13, No. 9, 1996.